

Horizontal Muons and a Search for AGN Neutrinos in Soudan 2

D. DeMuth^b, G. J. Alner^d, D. Ayres^a, W. L. Barrett^a, P. Border^b,
D. J. A. Cockerill^d, J. H. Cobb^c, H. Courant^b, T. Fields^a,
H. Gallagher^e, M. C. Goodman^a, R. Gran^b, T. Joffe-Minor^a,
T. Kafka^e, S. Kasahara^b, P. J. Litchfield^b, W. A. Mann^e,
M. Marshak^b, R. Milburn^e, W. Miller^b, L. Mualem^b, A. Napier^e,
W. Oliver^e, G. F. Pearce^d, E. Peterson^b, D. Petyt^b, K. Ruddick^b,
M. Sanchez^e, J. Schneps^e, A. Sousa^e, B. Speakman^b, J. Thron^a,
H.J. Trost^a, J. Uretsky^a, G. Villaume^b, N. West^c

^aArgonne National Laboratory, Argonne IL, USA

^bUniversity of Minnesota, Minneapolis MN, USA

^cUniversity of Oxford, Oxford, Oxon, UK

^dRutherford Appleton Laboratory, Didcot, Oxon, UK

^eTufts University, Medford MA, USA

Abstract

We measure the horizontal ($|\cos(\theta_z)| < 0.14$) neutrino-induced muon flux in Soudan 2 to be $3.81 \pm 0.47 \pm 0.29 \times 10^{-13} \text{ cm}^{-2} \text{ sr}^{-1} \text{ s}^{-1}$. From the absence of horizontal muons with large energy loss, we set a limit on the flux of muon neutrinos from Active Galactic Nuclei.

1 Introduction

The Earth provides an effective shield against the muon component of cosmic ray showers for overburdens exceeding 14,000 meters-water-equivalent (mwe). Consequently, near the horizontal direction ($|\cos(\theta_z)| < 0.14$) at the site of the Soudan 2 detector (vertical depth 2090 mwe), the muon flux is comprised almost entirely of μ^\pm initiated by charged current interactions of atmospheric muon neutrinos in the rock surrounding the detector. In addition, astrophysical neutrino sources may contribute to the (horizontal) muon flux. In particular, a high energy ($> 5 \text{ TeV}$) contribution may arise as the result of neutrinos which originate within astrophysical sources such as Active Galactic Nuclei (AGNs)[1,2,3,4,5,6,7].

Active galaxies are those with extreme variations in brightness corresponding to abnormal emission of large amounts of energy at optical and/or radio wavelengths. Colliding and exploding galaxies also fall into this category. The nuclei of these

galaxies may produce both neutral and charged particles. Most of the particles either decay or are absorbed before they can escape the galaxy, leaving only photons and neutrinos to be detected on Earth. Several models predict substantial high-energy neutrino production from AGNs[1,2,3,4,5,6,7], however there is a theoretical limit which conflicts with many of these models[8]. AGNs may collectively give rise to a diffuse neutrino flux, or they may be detectable as individual point sources. Gamma Ray Burst sources have also been proposed as another possible diffuse source of high energy neutrinos[9].

Charged current interactions of multi-TeV muon neutrinos ($\nu_\mu + \bar{\nu}_\mu$) in the rock surrounding the Soudan 2 detector can be expected to give rise to TeV muons at the detector. Muons with these large energies will very frequently exhibit catastrophic energy loss by bremsstrahlung or pair production as they traverse the tracking calorimeter. This is highly improbable for muons ($\langle E_\mu \rangle \sim 20$ GeV at the detector) initiated by atmospheric neutrino reactions in the surrounding rock. Thus it is possible to measure the rate of high energy AGN neutrinos.

In this paper we report a measurement of the horizontal muon flux of $3.81 \pm 0.47 \pm 0.29 \times 10^{-13} \text{ cm}^{-2} \text{ sr}^{-1} \text{ s}^{-1}$ and a negative search for high energy muons from AGNs.

2 The Soudan 2 Detector

The detector is located approximately 700 m below the Earth's surface in an historic iron mine in Soudan, Minnesota, USA. A photograph is shown in Figure 1.



Fig. 1. The Soudan 2 iron tracking calorimeter is a $8 \text{ m} \times 5 \text{ m} \times 16 \text{ m}$ assembly of standard-unit 4.3 ton modules. Each module contains corrugated Fe sheets interleaved with drift tubes and stacked into a fine-grained hexagonal lattice.

The central detector is an iron sampling calorimeter using drift tubes filled with 85% Ar - 15% CO_2 gas as the active medium.

The detector is made of 224 modules with dimensions of $2.7 \times 1 \times 1.1 \text{ m}^3$. Each module has a mass of 4.3 metric tons. The modules are stacked 2 high for a total height of 5.4 m, and 8 wide for a width of 8 m. The average density is 1.6 g/cm^3 .

The drift tubes are oriented along the North-South direction and are operated in proportional mode. Each end of the tubes is read out by an anode wire and a cathode pad which establish the x (East-West) and y coordinates of the hits. Off line, hits are matched in each half tube, using pulse height to match the cathode and anode

pulses. The z (North-South) position of the hit is determined by correlating the drift times.

The ceiling, floor, and walls of the detector hall are covered with an active shield consisting of a two layer aluminum proportional tube array. The shield array resolves charged particle crossings (“hits”) to within four microseconds and within rectangular surfaces of $10\text{ cm} \times 5\text{ m}$. For most Soudan 2 analyses, the shield is used to veto events in the main detector which were initiated by particles interacting in the surrounding rock. Use of coincident in-time shield hits in the present analysis is described in Section 4.

The trigger for recording events requires a multiplicity of seven anode pulses or eight cathode pulses in blocks of 16 contiguous readout channels. For long muon tracks this trigger is fully efficient.

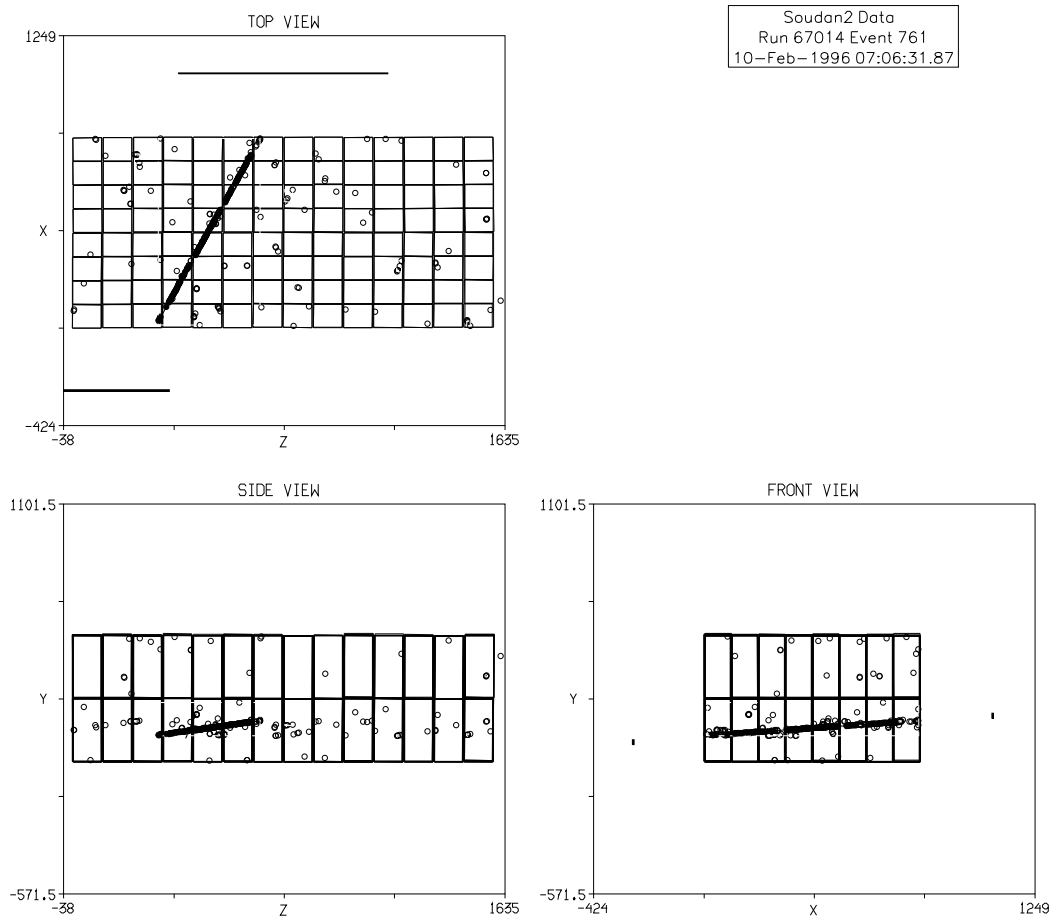


Fig. 2. Three views with correct aspect ratio of a neutrino-induced horizontal muon traversing the Soudan 2 detector. The muon traverses eight calorimeter modules. The proportional tube shield registers its entrance and exit points on the cavern walls (see Top and Front views). Dimensions are in cm, and individual module outlines are shown.

A near horizontal muon data event which is (presumably) neutrino-induced is shown

in Figure 2. This example is the longest horizontal muon track that was found, with a length of 1464 cm and 149 tube crossings used in the fit. The zenith (azimuth) angle of this track is 84° (23°). Two shield hits can be seen in the top and front views.

The construction and performance of the tracking calorimeter are extensively described in Reference [10].

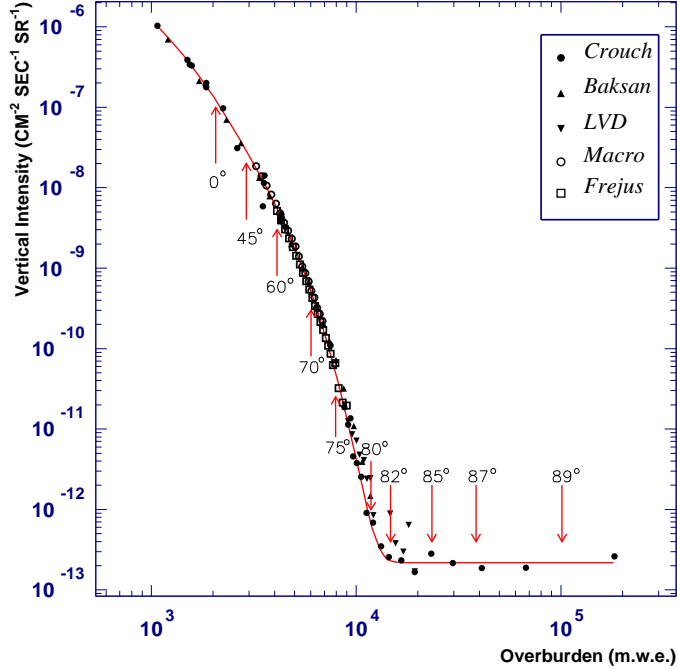


Fig. 3. The vertical muon intensity as a function of slant depth, from the compilation of M.F. Crouch[11,12]. Arrows indicate the average depth at different zenith angles (in degrees) at the Soudan 2 detector.

3 Horizontal Muons at Soudan 2

Figure 3 shows the vertical muon intensity underground as a function of depth in standard rock, as compiled by Crouch[11] and subsequently updated by the Particle Data Group[12]. Two distinct components are apparent in the fitted curve, which consists of a double exponential plus a constant term. The atmospheric muon rate is observed to fall sharply with slant depth, so that the flatter spectrum of neutrino-induced muons only becomes visible for slant depths greater than 14 kmwe. For angles θ_z with respect to the vertical (zenith angle), the slant depth increases approximately as $\sec(\theta_z)$, but depends in detail on both the surface terrain and the rock density and composition.

Based on the vertical muon spectrum and the calculation of the average slant depth at Soudan 2 as shown in Figure 3, we can select a sample of neutrino induced muons by making a cut on the zenith angle near 82° . Since the event timing resolution is about 100 ns, it is not possible to ascertain whether a muon is upward- or downward-going. There is thus a two-fold ambiguity in the direction for each measured track and θ_z is defined to be $\leq 90^\circ$.

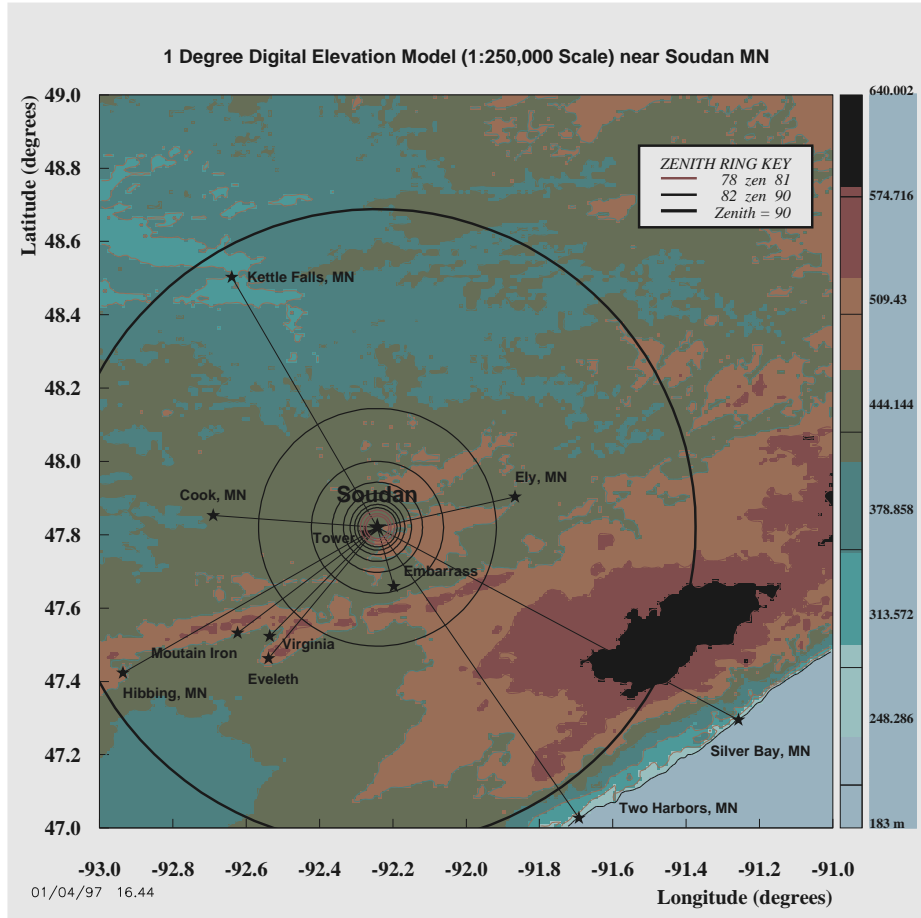


Fig. 4. USGS 1 degree digital elevation model extending to Lake Superior. The zenith angles $78 \leq \theta_z \leq 90$ are projected onto the surface. The distance between Soudan and Two Harbors, MN, is 97 km.

Calculation of the slant depth requires knowledge of both the rock density and the surface terrain. Differences between standard rock ($\rho \sim 2.62 \text{ g/cm}^3$) and Soudan rock ($3.00 \text{ g/cm}^3 > \rho > 2.74 \text{ g/cm}^3$) must be taken into account. The topology above and surrounding the Soudan site is shown in Figure 4[13]. The geology of the region is such that the iron deposits are almost vertical, so that the most vertical zenith angles correspond to the highest average density. The majority of the rock is greenstone composed of silicon dioxide (SiO_2) and aluminum oxide (Al_2O_3). [14] Based on Soudan rock effective parameters, a depth of 14 kmwe in standard rock corresponds to 13.2 kmwe in Soudan rock.[15]

Due to the uneven surface terrain, the slant depth was calculated for each track

individually. Observed fluxes of cosmic ray induced muons with $\theta_z < 60^\circ$ have been used to determine the zenith angle dependence of the rock density[16]. By considering the azimuthal variation in the slant depth, we infer that systematic uncertainties in the atmospheric muon flux due to incomplete knowledge of the rock density are on the order of 10%.

Upon inclusion of the terrain information, a more refined estimation of the slant depth as a function of zenith angle is obtained, as indicated in Figure 5. The solid curve in that Figure was made assuming a spherical Earth. The dots which appear each one degree in zenith (two degrees in the inset) and are averaged over ten degrees in azimuth reflect the effect of topology variations in the overburden.

	Data Selection Criteria
1	Track Status (extra-fiducial detector hits and in-time shield hits)
2	Track Length Cut (> 175 cm)
3	Azimuthal Cut ($> 8^\circ$ from quadrant axis)
4	Zenith Cut ($\geq 78^\circ$)
5	Anode Width

Table 1
Selections used to define the horizontal muon sample.

4 Reconstruction of Neutrino-Induced Muon Tracks

There were approximately 10^8 triggered events in the Soudan 2 detector in the data set considered for this analysis. About half of these were due to cosmic ray muons, and half due to radioactivity in different parts of the detector which satisfied the trigger due to multiplexing. These events were processed using a pattern recognition filter code which identifies muon tracks and discriminates against unphysical background from noise[15]. Five additional cuts were then applied to define a “horizontal muon” sample as listed in Table 1.

Tracks were required to have end points consistent with a particle entering and leaving the detector. Acceptable track ends were required to (1) lie outside the fiducial volume which is 50 cm from the edge of the main detector, or (2) lie on a module boundary inside of the main detector and (3) point to a coincident shield hit or (4) point to a portion of the shield where a shield module did not exist. The azimuth cut rejected noise events which reconstructed parallel to the axes of the detector. A zenith cut defined the sample of horizontal muons. A track length cut minimized short tracks such as pions that originated from nuclear interactions within the rock nearby and also low energy cosmic ray muons which had undergone large multiple Coulomb scattering.

The anode-width cut rejected events that were primarily along one anode wire. These were actually along the north-south direction in azimuth, but they were often misreconstructed. The efficiency of these cuts for Monte Carlo muons generated isotropically with zenith angles exceeding 82 degrees is 0.56 ± 0.01 as given in Table 2. Note that both the trigger and reconstruction efficiency are lower near zenith angles of 90 degrees.

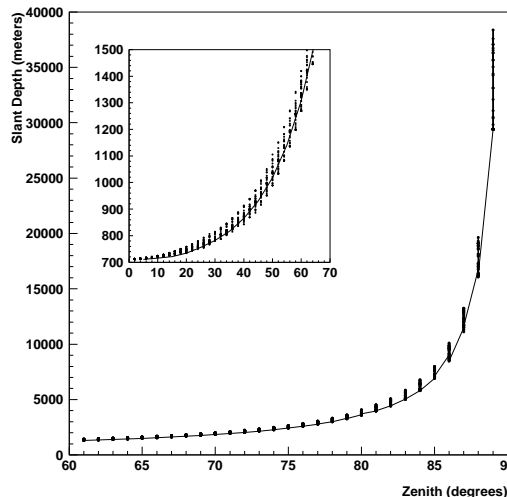


Fig. 5. Estimation of slant depth versus zenith angle for a spherical Earth (curve) and upon inclusion of terrain and density information for the Soudan site (dots).

The pattern recognition software found single horizontal muon tracks, but it also kept a variety of background events. Most background events contained short horizontal tracks accompanied by other activity in the detector. Physicist scanning of all tracks greater than 78° was done to verify the track fits and to eliminate obvious backgrounds. Common backgrounds were due to certain patterns of electronic noise, vertical muons undergoing large radiative stochastic losses, multiple muons, and neutrino interactions within the detector. Tracks with visible multiple scattering (greater than 2 degrees) or with in-time shield hits that were not due to a horizontal muon were also rejected. All events were subjected to two independent scans and residual discrepancies were rescanned. The scan rejected 58% of data events output from the filter. The uncorrelated scan inefficiency as determined from the double scan was less than 1%. The scan efficiency was calculated to be 95%. The dominant loss was due to multiple scattering by more than 2° within the Soudan 2 detector by those muons with the lowest energies.

The track-length cut of 1.75 m (2.2 hadronic interaction lengths) minimized the number of short tracks which arose from processes which were not neutrino-related. The latter backgrounds included pion tracks originating from deep inelastic muon scattering within nearby rock, or else high energy cosmic ray muons from vertical directions which experienced large-angle multiple scattering. This length corresponds to a muon energy threshold of 400 MeV, but the restriction on multiple scattering raised this to an effective threshold of 1.8 GeV.

The number of accepted events after scanning, with $\theta_z > 78^\circ$, was 1237 events. The slant depth cut of 14 kmwe reduced this sample to 65 events. The track length, azimuth and zenith angle distributions of all 1237 events are shown in Figure 6. Figure 7 shows the (θ_z, ϕ) distribution of these events. The depletions at regular intervals on azimuthal projections of these plots are 'due to the azimuth cuts. The

Cut	
Generate	2000
Matched Track	1920
Track Status	1818
Track Length	1685
Azimuth	1411
Zenith	1378
Anode-width	1111
ϵ	55.6%

Table 2

Survival rates through selections of this analysis for Monte Carlo muons incident from near horizontal directions.

wavy-line contour on Figure 7 shows the 14 kmwe slant depth cut, which is designed to separate the sample into atmospheric muon and neutrino-induced muon candidates. The event with the largest slant depth is shown in Figure 8.

To estimate the amount of background from atmospheric muons we integrate under the intensity-vs.-slant-depth curve of Figure 3, but without the constant (neutrino-induced muon) term, for slant depths greater than 14 kmwe. This procedure yields a background estimate of $0.1^{+0.2}_{-0.1}$ events in our horizontal muon sample, where the error reflects the uncertainty in the rock density.

Muons which multiple scatter in the Earth above the Soudan 2 detector are a potential source of additional background. Since the overburden above the Soudan 2 detector is so great, it is not appropriate to apply the usual equation for small angle multiple scattering. Instead, a Monte Carlo calculation was performed which propagated muons through the Earth and calculated the energy loss in steps. With a sample starting with the same number of muons with $\theta_z > 60$ degrees at the surface of the Earth, no additional muons were generated with $\theta_z > 82$ degrees at the detector. The finite statistics of the Monte Carlo introduced an additional uncertainty which corresponds to < 0.5 event background. We conclude that the expected background is less than one event.

As a consistency check we note that if multiple scattering of cosmic ray muons were a source of significant background, there should be evidence of excess events with short track length, as it would be unlikely that a muon which had scattered through a large angle could make a long track in the detector without undergoing additional visible scattering. A comparison of the track length distribution of the data and the neutrino-induced Monte Carlo showed no evidence for additional events with short path lengths.

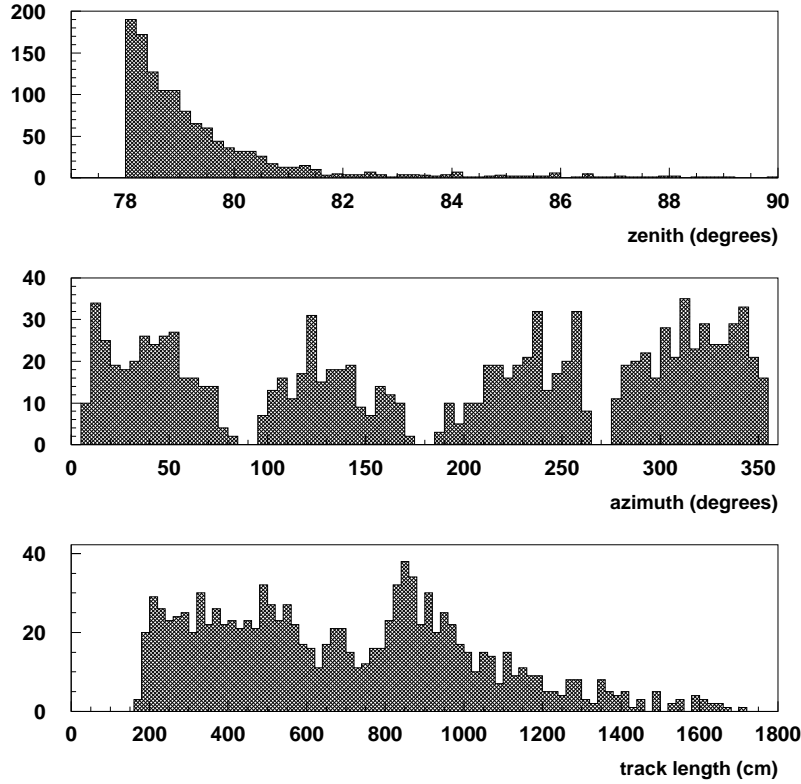


Fig. 6. The reconstructed zenith, azimuth and track-length distributions for through-going muons which were selected by the filter software to have a zenith in excess of 78° and passed the scan criteria. The shape of the track-length distribution reflects the shape of the detector for an isotropic muon flux.

The neutrino-induced muon flux, Φ_μ , can be expressed as

$$\Phi_\mu = \frac{N_\mu}{t A \Omega \varepsilon} \quad (1)$$

where t is the time exposure of the detector in seconds, A is the effective area of the detector in cm^2 , Ω is the solid angle subtended by the detector in steradians, and ε is the detection efficiency for the muons in the detector. Both A and Ω are calculated assuming a uniform acceptance to the right of the contour in Figure 7.

The analyzed data spanned the period from April 14, 1992 to April 24, 2002. The exposure time was calculated from the start and end times of every processed data run. The calculated exposure for this analysis, including corrections for the detector duty cycle and electronics dead time during data taking, is 2.00×10^8 s. To estimate the effective area for this analysis, Monte Carlo muons were uniformly generated and the effective area for each track calculated. For zenith angles greater than 78° the average area was 90.6 m^2 . For $\theta_z > 82^\circ$ the average effective area was $86.7 \pm 0.3 \text{ m}^2$. The solid angle was calculated from the acceptance region in Figure 7 to

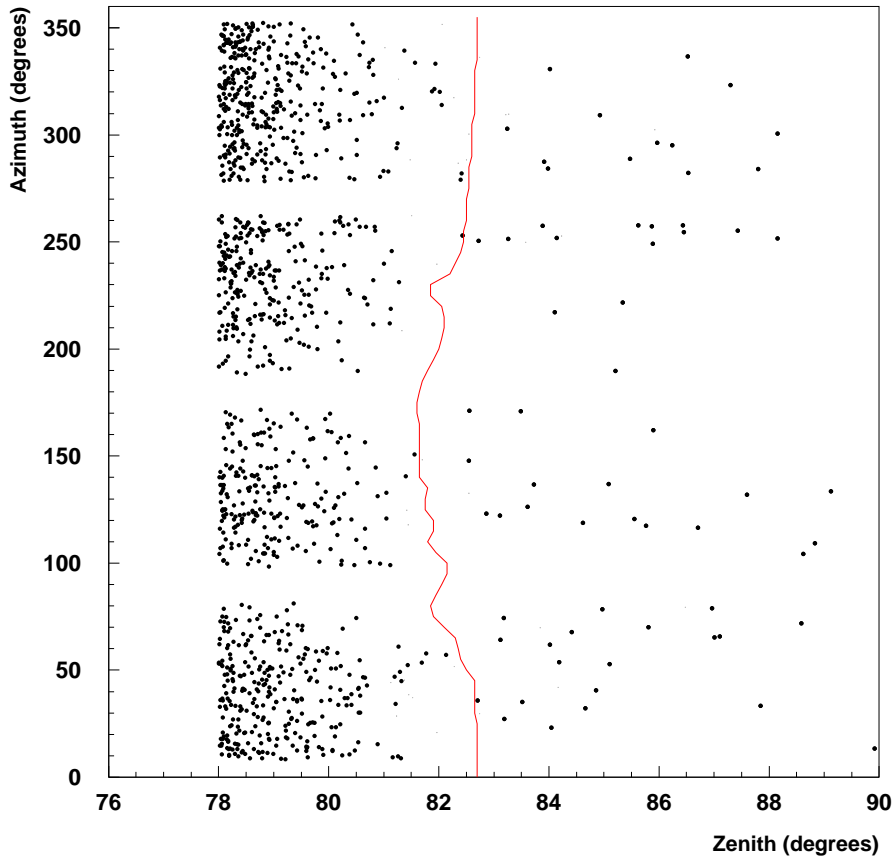


Fig. 7. Angular distribution of horizontal muon candidates. The contour line near $\theta_z = 82^\circ$ represents the 14 kmwe contour.

be 1.77 sr. The trigger and reconstruction efficiency $\varepsilon = 0.53$ (0.56 from Table 2 \times 0.95 from scanning.)

Systematic errors arise with the uncertainty in the background of 0.7 events (1%), uncertainties in the scan efficiency (5.6%) and uncertainty in the energy distribution as it affects the efficiency of the 2° multiple scattering cut (5%). Adding these errors in quadrature, we assign an overall systematic uncertainty to the neutrino flux calculation of 7.6%.

The resulting neutrino-induced muon flux is

$$\Phi_{\nu_\mu} = 3.81 \pm 0.47(stat) \pm 0.29(sys) \times 10^{-13} \text{ cm}^{-2} \text{ sr}^{-1} \text{ s}^{-1} \quad (2)$$

Upward-going atmospheric neutrino-induced muons have been previously measured by Baksan, IMB, MACRO, Kamiokande, and Super-Kamiokande[17,18,19,20,21].

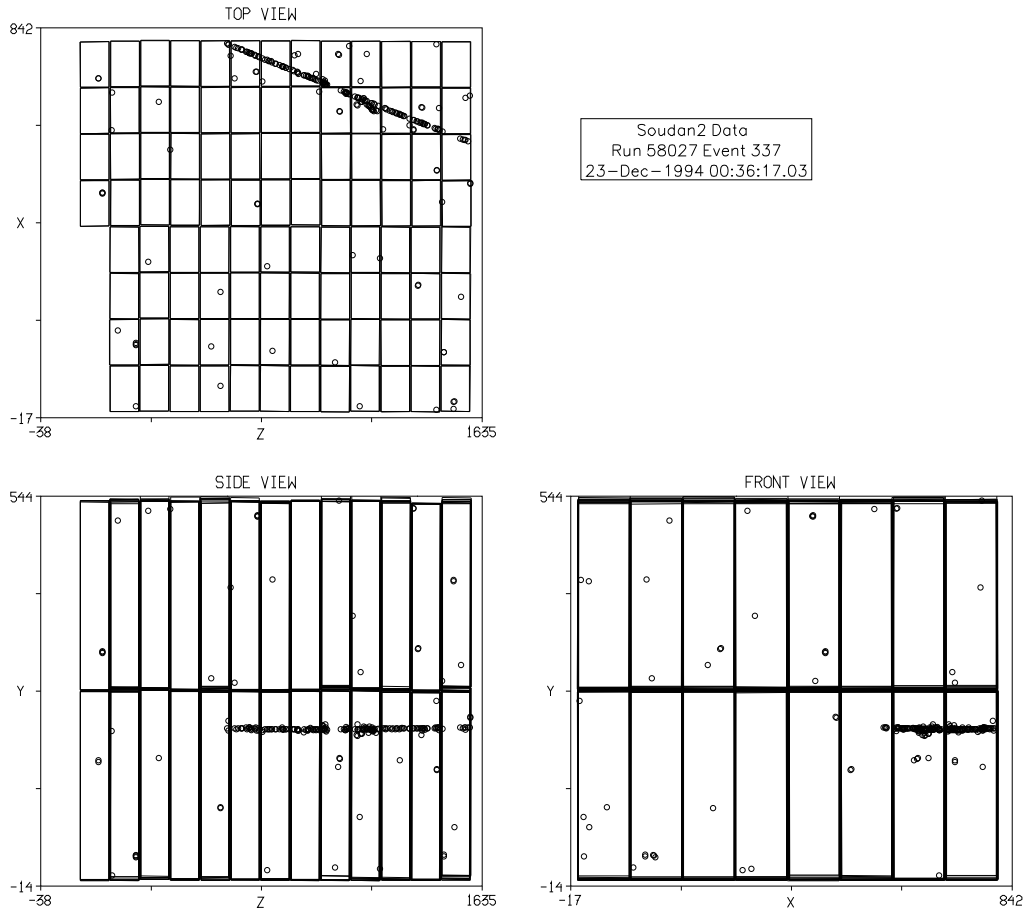


Fig. 8. Our largest zenith angle event. $\theta_z = 89.9^\circ$ and the length is 731 cm. The scales are labeled in cm.

However, these experiments have not reported neutrino-induced muon fluxes above the horizon from those regions of solid angle where the overburden might be sufficient to separate atmospheric muons, perhaps due to uncertainties in the topology and density. The SNO experiment is deep enough that it should be able to see the neutrino-induced muon flux above the horizon[22]. The flux near the horizon has also been measured by LVD and Frejus[24,23]. The present measurement has aspects in common with that of Frejus, albeit with increased statistics. LVD, which has a much less uniform overburden, did not separate their neutrino-induced signal from background. The measured fluxes closest to $\theta_z = 90^\circ$ are tabulated in Table 3 along with our estimate of the muon energy threshold used for each analysis.

Super-Kamiokande, and Kamiokande, MACRO, and Soudan 2 as well [25,28,26,27] have analyzed atmospheric neutrino events and concluded that neutrino oscillations modify the zenith angle distribution of the ν_μ flavor component of the atmospheric neutrino flux. For a neutrino energy of 40 GeV and assuming $\Delta m^2 \sim 3.5 \times 10^{-3} \text{ eV}^2$ and maximal (θ_{23}) mixing, the probability of oscillation for a ν_μ from 82°

Experiment	Flux ($10^{-13}\text{cm}^{-2}\text{sr}^{-1}\text{s}^{-1}$)	E_{min} (GeV)	$\cos \theta_z$
Baksan[17]	3.72	1	-0.1 to 0.0
Frejus[23]	3.67 ± 0.66	0.3	-0.18 to 0.18
LVD[24]	8.3 ± 2.6	1.0	-0.1 to 0.1
IMB[18]	5.66 ± 0.95	1.8	-0.14 to 0.0
Kamiokande[20]	2.84 ± 0.53	1.7	-0.1 to 0.0
Super-Kamiokande[21]	3.45 ± 0.33	1.6	-0.1 to 0.0
MACRO[19]	7.4 ± 2.8	0.4	-0.1 to 0.0
Soudan 2	3.81 ± 0.64	1.8	-0.14 to 0.14

Table 3

Comparison of near-horizontal neutrino-induced muon fluxes measured by several experiments.

($\langle L \rangle \sim 130$ km) is 2.1×10^{-4} while for a ν_μ from 98° ($\langle L \rangle \sim 2000$ km) it is 0.04. Our modest statistics and $90^\circ - \theta_z$ ambiguity make an oscillation analysis of these events impractical.

5 AGN Neutrino Search

Several models for neutrino production in Active Galactic Nuclei predict large and potentially measurable fluxes of very high energy neutrinos[1,2]. These neutrinos would then produce high energy muons with energies from a few TeV up to 100's of TeV. In this energy range the dominant energy loss process for the muons in iron is electron pair production, followed by bremsstrahlung[29]. Both processes produce large electromagnetic showers in the Soudan 2 detector which are easily detected and measured.

To understand the response of the tracking calorimeter to these TeV muons, a simulation was performed. High energy muons were propagated through the Soudan 2 detector and the amount of energy they deposited was calculated in a GEANT-based Monte Carlo[30]. Three different muon energies were studied: 5, 20 and 100 TeV. Figure 9 shows the fraction of muons which lost at least a specific amount of energy versus that energy loss for three different muon energies. The results obtained from the simulation agree with an analytic calculation carried out independently[31]. While 60% of the 5 TeV muons lose 5 GeV or more, 91% of the 20 TeV muons and 99% of the 100 TeV muons lose at least 5 GeV in the detector.

The muons identified for the horizontal muon flux measurement were subjected to a predetermined cut of 5 GeV on the amount of energy loss they experienced in the

detector. None of the 65 events had visible radiated energy loss greater than this cut. The largest zenith angle event with substantial visible energy loss is shown in Figure 10. This event has a horizontal muon with a zenith angle of 80.6° and an azimuthal angle of 133° which entered the top of the detector and exits the north wall. Parallel to the muon at the top is an entering electromagnetic shower, presumably from a bremsstrahlung or pair production process along the muon path in the rock above the detector. From Figure 7, the zenith angle (80.6°) tags the event as a high energy cosmic ray muon and not a horizontal muon candidate. Visible energy loss from a cosmic ray muon is not unexpected, because for atmospheric muons at the detector near zenith angle 80° , $\langle E_\mu \rangle \sim 380$ GeV while for atmospheric neutrino induced muons, $\langle E_\mu \rangle \sim 20$ GeV. The energy of the shower is reconstructed to be 2.2 GeV. There are no such events among the 65 horizontal muon candidates.

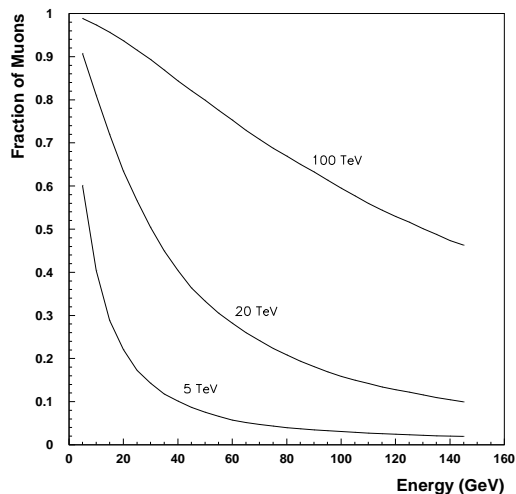


Fig. 9. Calculation of non-ionization energy loss for muons in Soudan 2

Models for neutrinos from AGNs predict a ν flux as a function of energy. For each assumed functional form of the predicted neutrino energy spectrum, an observation or limit on high energy muons can be used to normalize or limit the neutrino flux. It is less meaningful to plot a limit on a neutrino energy distribution for an arbitrary functional form. Therefore we choose to show our limit on the neutrino-induced muon energy distribution. For each muon energy, our non-observation of events with energy loss corresponds to an upper limit on the muon flux.

To provide a comparison of our search with other searches reported in the literature, we show in Table 4 the exposures ($A \times t \times \Omega \times \varepsilon$). Our exposure is larger than that of the Frejus experiment, but lower than MACRO or AMANDA. Since the latter two experiments focus on upward-going muons, and the Frejus and Soudan 2 limits use horizontal muons, the limits are complementary for the exotic case involving the highest energy neutrinos for which the Earth's neutrino opacity is large ($E_\nu > 50$ TeV)[9].

Based upon the observation of zero events, together with our efficiencies, we calculate 90% CL upper limits for the integral muon flux above three energies, which are shown in Table 5 and Figure 11. Our limit is close to the highest predicted flux; however that flux is not ruled out. The limits are lower for higher energy cut-offs

Experiment	Exposure (10^{14} cm ² s sr)
Soudan 2	1.71
Frejus	1.60
MACRO	3.40
AMANDA	13.9

Table 4

Comparison of exposures (Product of running time, effective area, solid angle and efficiency) for AGN neutrino search experiments

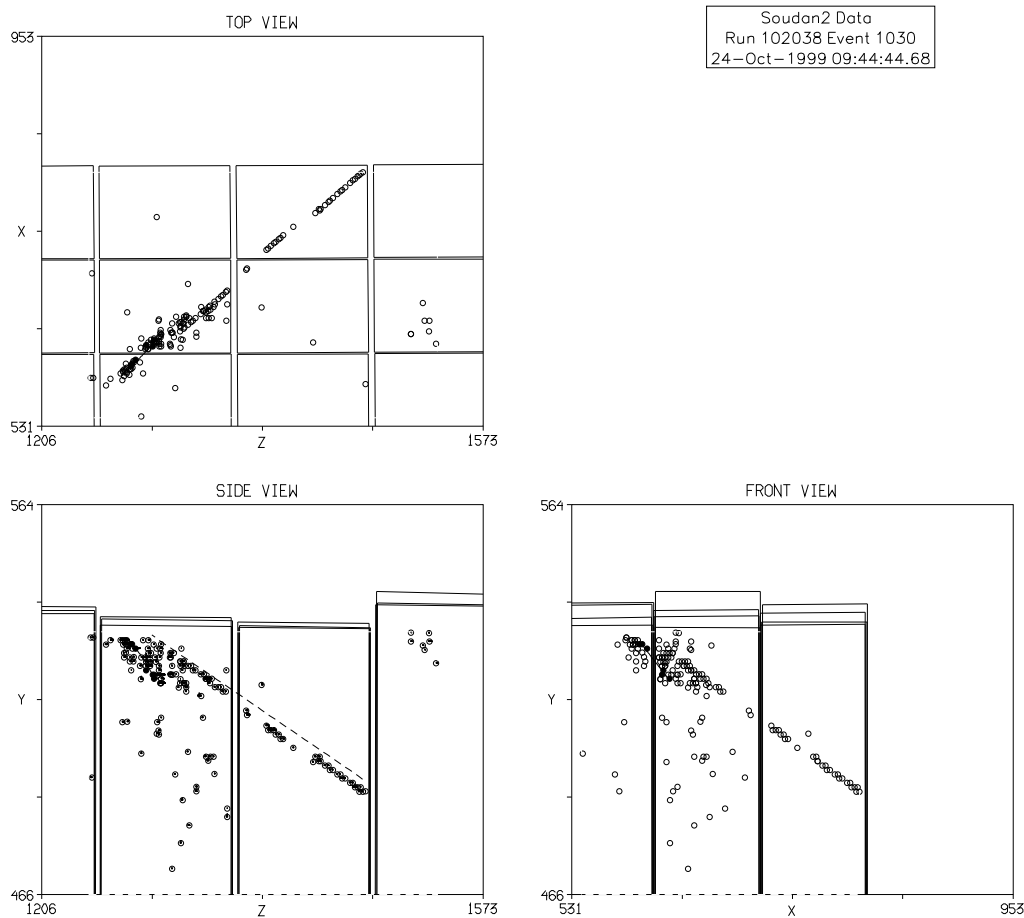


Fig. 10. Views of the muon event of largest zenith angle (80.6°) having a substantial radiative energy loss. The muon's zenith angle is too small to qualify as a neutrino-induced candidate. The vertical scale is magnified and all scales are labeled in cm.

because of the higher probability of detecting a large energy loss.

Other experiments have also used their horizontal muon events to set limits on the flux of the diffuse AGN neutrinos. The Frejus experiment used two methods to set a limit on the flux of high energy neutrinos[32]. One method extrapolated a fit to

Soudan 2 Flux Limits for AGN Neutrinos

Energy (TeV)	High Energy μ Efficiency	90% CL Limit ($\text{cm}^{-2}\text{sr}^{-1}\text{sec}^{-1}$)
5	60%	2.2×10^{-14}
20	91%	1.5×10^{-14}
100	99%	1.4×10^{-14}

Table 5

Efficiency for high energy muons to experience at least 5 GeV energy loss in the Soudan 2 detector and the resulting AGN neutrino flux limits.

the atmospheric neutrino energy spectrum obtained previously[23]. Since that fit assumed that one spectral index fit all of their data, using it to deduce a limit for muons arising from a different energy distribution may bias that limit toward small values. The limit was quoted as $d\phi/dE_\nu(2.6 \text{ TeV}) < 7.0 \cdot 10^{-13} \text{GeV}^{-1} \text{cm}^{-2} \text{s}^{-1} \text{sr}^{-1}$. With their second method, Frejus used the absence of muons with large energy loss to constrain the normalization of a number of specific models of the high energy neutrino flux[32].

The MACRO experiment[33] conducted an AGN search and found 2 candidate events with background of 1.1 expected. They set an upper limit on the muon flux from diffuse neutrinos of $(1.7 \pm 0.2) \times 10^{-14} \text{cm}^{-2} \text{s}^{-1} \text{sr}^{-1}$. Their efficiency was highest for upward-going muons and lowest for horizontal muons. The AMANDA neutrino telescope, located in the ice near the South Pole, has set a limit based on an assumed diffuse E_ν^{-2} spectrum of $dN/dE_\nu \leq 10^{-6} E_\nu^{-2} \text{cm}^{-2} \text{s}^{-1} \text{sr}^{-1} \text{GeV}^{-1}$ [34]

As another test for an extraterrestrial component in the horizontal muon events, we have examined them for evidence of point sources. Figure 12 shows the directions of the 65 horizontal muons in galactic coordinates using an Aitoff projection of the galaxy. For each muon, the two possible directions are plotted. We observe that no clusters involving two or more muons within the detector’s angular resolution ($0.3^\circ \times 0.3^\circ$)[35] appear within the plot.

6 Summary

In this study we have isolated a sample of 65 neutrino-induced muon candidates, with an estimated background of less than one event. This corresponds to a muon flux of $3.81 \pm 0.47^{stat} \pm 0.29^{sys} \times 10^{-13} \text{cm}^{-2} \text{sr}^{-1} \text{s}^{-1}$ in the horizontal direction $-0.14 < \cos \theta_z < 0.14$. None of the 65 events have a large energy loss in the detector. We set an integral limit on neutrino-induced muons from AGNs and/or other sources from between 1.4 and $2.2 \times 10^{-14} \text{cm}^{-2} \text{sr}^{-1} \text{s}^{-1}$ depending on muon energy.

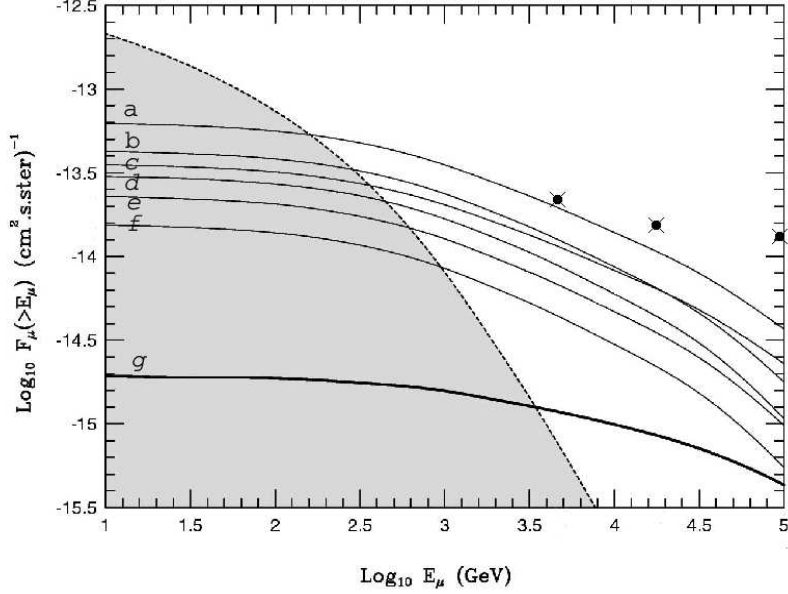


Fig. 11. The data points are our totally correlated limits from Table 5. The Curves a-f are from horizontal muon flux predictions from models by Szabo and Protheroe [2] and curve g from Stecker [5]. The shaded area represents the atmospheric neutrino flux.

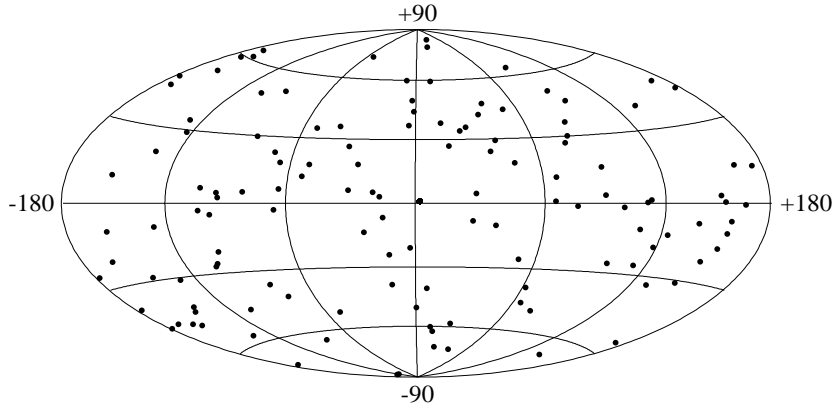


Fig. 12. Aitoff Projection of the 65 horizontal muon candidates. Each event has two projections due to the ambiguity in direction.

7 Acknowledgments

We thank Rick Egeland, Leah M. Goodman and Adrian Ryerson for their help in this analysis. This work was supported by the U.S. Department of Energy, the U.K. Particle Physics and Astronomy Research Council, and the State and University of Minnesota. We also wish to thank the Minnesota Department of Natural Resources for allowing us to use the facilities of the Soudan Underground Mine State Park.

References

- [1] F.W. Stecker et al., Phys. Rev. Lett., 66 (1991) 2697.
- [2] A.P. Szabo and R.J. Protheroe, Astropart. Phys. 4 (1994) 375.
- [3] R.J. Protheroe and D. Kazanas, Astrophys. Journ. 265 (1983) 620.
- [4] F.W. Stecker, O.C. DeJager and M.H. Salamon, Astrophys. Journ. 390 (1992) L49.
- [5] F.W. Stecker et al., Phys. Rev. Lett. 66 (1991) 2697.
- [6] T.K. Gaisser, F. Halzen and T. Stanev, Phys. Rep. 258 (1995) 173.
- [7] K. Mannheim, Astropart. Phys. 3 (1995) 295.
- [8] E. Waxman and J. Bahcall, Phys. Rev. D59 (1998) 023002.
- [9] F. De Paolis et al., Astropart. Phys. 18 (2002) 249.
- [10] W.W.M. Allison et al., Nucl. Inst. Methods A 376 (1996) 36; W.W.M. Allison et al., Nucl. Inst. Methods A 381 (1996) 385.
- [11] M.F. Crouch, Proceedings 20th ICRC, Moscow USSR, 1987, 6 165.
- [12] Review of Particle Physics, Eur. Phys. J. C 15 (2000) 153.
- [13] U.S. Department of the Interior, US Geological Survey, Office of Data and Information Delivery, 508 National Park Center, Reston VA 20192.
- [14] P.H. Sims and G.B. Morey, eds, "Geology of Minnesota", MN Geo Survey, 1972, and A Ruotsala, "Chemical Analyses of Igneous Rocks", MN Geo Survey, 1975.
- [15] D.M. DeMuth, Ph.D. thesis, University of Minnesota, (1999) (<http://www.umn.edu/~demuth/thesis/>).
- [16] Keith Ruddick, Sudan 2 internal note PDK-435 (1990) (unpublished); S.M. Kasahara, Ph.D. thesis, University of Minnesota, (1997).
- [17] M. M. Boliev et al., Proceedings 3rd Int. Workshop on Neutrino Telescopes (ed. M. Baldo Ceolin) (1991) 235.
- [18] R. Svoboda et al., Astrophys. J. 315 (1987) 315.
- [19] M. Ambrosio et al., Phys. Lett. B434 (1998) 451.
- [20] M. Mori et al., Phys. Lett. B270 (1991) 89.
- [21] Y. Fukuda et al., Phys. Lett. B467 (1999) 185; A. Habig, hep-ex/9903047.
- [22] A. McDonald, Nucl. Phys. B(Proc. Suppl.) 91 (2001) 21.
- [23] K. Daum et al., Z. Phys. C66 (1995) 417.
- [24] M. Aglietta et al., Astropart. Phys. 3 (1995) 311.

- [25] Y. Fukuda et al., Phys. Rev. Lett. 81 (1998) 1562.
- [26] K.S. Hirata et al., Phys. Lett. B280 (1992) 146.
- [27] S. Ahlen et al., Phys. Lett. B357 (1995) 481.
- [28] W.W.M. Allison et al., Phys. Lett. B391 (1997) 491.
- [29] W. Lohmann, R. Kopp and R. Voss, CERN Report 85-03 (1985).
- [30] M. Goodman et al., Proceedings of High Energy Neutrino Astrophysics Workshop, Univ. of Hawaii, ed. V.J. Stenger et al., World Scientific, Singapore (1992) 243.
- [31] J. Uretsky, Nucl. Inst. Meth. A 399 (1997) 285.
- [32] W. Rhode et al., Astropart. Phys. 4 (1996) 217.
- [33] M. Ambrosio et al., astro-ph/0203181, to appear in Astropart. Phys.; F. Ronga for the MACRO Collaboration, Nucl. Phys. B 77 (1999) 117.
- [34] E. Andres et al., Nucl. Phys. Proc. Suppl. 91 (2000) 423.
- [35] J.H. Cobb et al., Phys. Rev. D61 (2000) 092002.